Temporary topological trapping and escape of charged particles in a flux tube as a cause of delay in time asymptotic transport

P. Tooprakai,[1,2,3] P. Chuychai,[2] J. Minnie,[2] D. Ruffolo,[3] J. W. Bieber,[2] and W. H. Matthaeus[2]

Received 11 May 2007; revised 20 July 2007; accepted 8 August 2007; published 14 September 2007.

[1] The scenario of temporary trapping of magnetic field lines and their subsequent suppressed diffusive escape from topological magnetic structures embedded in turbulence has been offered as a way to understand the persistence of "dropouts", or sharp gradients in observed heliospheric energetic particle intensities. Here a set of numerical experiments is carried out to show the basic physics of this process: charged test particles can be temporarily trapped in flux tubes and then escape due to random turbulent perturbations in the magnetic field. The overall effect is a delay in the onset of time-asymptotic transport. We thus confirm that previous arguments based on field line transport are also applicable to test particle transport.
Citation: Tooprakai, P., P. Chuychai, J. Minnie, D. Ruffolo, J. W. Bieber, and W. H. Matthaeus (2007), Temporary topological trapping and escape of charged particles in a flux tube as a cause of delay in time asymptotic transport, *Geophys. Res. Lett.*, *34*, L17105, doi:10.1029/2007GL030672.

1. Introduction

[2] Populations of energetic particles observed in the heliosphere are described frequently using transport equations that incorporate diffusion in an essential way. The standard view is that spatial transport of an ensemble of charged particles involves two types of diffusion – parallel diffusion along and perpendicular diffusion across the mean local magnetic field [*Jokipii*, 1966]. To these additional effects such as convection, adiabatic expansion and local acceleration may be added to formulate a complete transport theory [*Parker*, 1965]. This type of transport theory has been successful to the degree that it is tempting to regard the approach as fundamental. There are however problems, especially for perpendicular transport, the most serious of which are observational. As an example, heliospheric energetic particle observations seem to require rapid cross field transport over large expanses of latitude in Ulysses observations [*McKibben et al.*, 2001]. On the other hand the persistence of sharp gradients in the observed flux of solar energetic particles, known as dropouts, seems to set an upper limit on cross field diffusion that is much lower than what is needed to account for latitudinal transport [*Mazur et al.*, 2000]. Evidently, to account for these observed features, one must take in to account factors not ordinarily included in standard diffusive transport theory. These include time dependence of the heliospheric field lines at their base [*Fisk*, 1996; *Giacalone et al.*, 2000] and topological trapping associated with turbulent flux tube structure transverse to the large scale heliospheric magnetic field [*Ruffolo et al.*, 2003; *Chuychai et al.*, 2005, 2007]. Here we further explore the second of these ideas, examining whether charged particles as well as magnetic field lines might experience effects associated with the magnetic field topology of the homogeneous turbulence in which their transport is initiated.

[3] The usual sequence of events in transport is that particles (or field lines) initially stream freely, and then begin to be affected by a random force. Once the random force is sampled over its correlation length (or time) the process of random walk, or diffusion, becomes evident. A well known difficulty arises when the magnetic irregularities responsible for diffusion have reduced dimensionality [*Jokipii et al.*, 1993; *Jones et al.*, 1998], so that diffusion might not occur at all, or perhaps it can only be recovered by defining a suitably designed ensemble. A further difficulty in arriving at a time-asymptotic transport limit (diffusive or not) is that certain subsets of particles with special initial or boundary conditions might require different times to relax to the statistical state, meanwhile retaining memory of the initial state. In this way the pre-diffusive epoch of single particle transport (ordinarily associated with free streaming) might persist for widely varying times, for specially prepared subensembles of particles. Therefore, for example, diffusion might be a good approximation when averaged over all energetic particles in the heliosphere, but might not apply to particles from a particular solar flare as observed at Earth orbit.

[4] The basic idea explored here originates in a careful examination of magnetic flux surfaces in so-called two-component turbulence models. These are a composite of two ingredients – slab (1D) fluctuations that vary only along the (uniform) mean magnetic field direction, and two-dimensional (2D) fluctuations that vary only in the two perpendicular directions [e.g., *Bieber et al.*, 1994]. The superposition of the two types of fluctuations is fully three dimensional (3D) even though the separate components are of reduced dimensionality. Field line trajectories in large amplitude fluctuations of this type [*Matthaeus et al.*, 1995] are well described by diffusion theory, for displacements greater than a few correlation lengths along the mean field, provided that averages are taken over an unbiased random sampling of field lines. However a closer inspection [*Ruffolo et al.*, 2003] reveals that diffusive transport can

[1]Department of Physics, Faculty of Science, Chulalongkorn University, Bangkok, Thailand.
[2]Department of Physics and Astronomy and Bartol Research Institute, University of Delaware, Newark, Delaware, USA.
[3]Department of Physics, Faculty of Science, Mahidol University, Bangkok, Thailand.

0094-8276/07/2007GL030672$05.00

Table 1. Particle Parameters for $B_0 = 5$ nT and $\lambda = 0.02$ AU and Simulated/Calculated Arrival Time of the Particles at the First Peak

						Time to First Peak[a]		
	Energy, MeV	$\|\mathbf{v}\|$, c	r_L, λ	r_L, AU	α	Low B	Medium B	High B
low E	0.02	0.0065	0.00136	2.73×10^{-5}	4.780	2000/1254	240/271	200/183
medium E	0.10	0.0146	0.00305	6.11×10^{-5}	4.779	600/560	98/121	62/82
high E	1.00	0.0461	0.00966	1.93×10^{-4}	4.775	200/177	38/38	20/26

[a]The first number is the simulated time, and the second number is the calculated time. Units are λ/c.

be greatly delayed for a subset of field lines that begins in the vicinity of O-type neutral points of the 2D fluctuations. This delay is due to the confining topology of the flux tube along with suppressed diffusive escape where the 2D field is strong [*Chuychai et al.*, 2005]. A single 2D flux tube provides a useful model of both contributions to the field line trapping near O-type structures that naturally occur at random locations in 2D turbulence [*Chuychai et al.*, 2007]. If particles injected near O-points experience delays similar to those of the field lines, that may explain the dropouts in solar energetic particles.

[5] We propose that charged particles can experience delays in perpendicular transport associated with the initial magnetic topology into which they are injected. To examine this conjecture, we will examine test particle experiments in which the O-type structure of the transverse fluctuating magnetic field is represented by a single two-dimensional magnetic flux tube with a Gaussian profile, sufficiently small that it does not affect other plasma properties. The rest of the system is the very simple case of a uniform DC magnetic field, on which is superposed a statistically uniform field of magnetostatic 1D slab turbulence that also permeates the flux tube. The results confirm our basic conjecture that temporary trapping leads to a delay in perpendicular transport and the formation of steep perpendicular gradients in an initially localized particle distribution. Trapping is more effective for stronger flux tubes and lower energy test particles.

2. Model and Methods

2.1. Equation of Motion

[6] To evaluate particle trajectories, we numerically solve the Newton-Lorentz force equation in a set of units for which all quantities as scaled to the mean magnetic field (B_0), the speed of light (c), the slab turbulence coherence length (λ), and the time scale $\tau_0 = \lambda/c$. The equations of motion become

$$\frac{d\mathbf{v}'}{dt'} = \alpha(\mathbf{v}' \times \mathbf{B}') \tag{1}$$

where $\alpha = (qB_0\tau_0)/(\gamma m_0)$ and $\mathbf{v}'$, $\mathbf{B}'$, and t' are normalized quantities.

2.2. Magnetic Field Model

[7] The magnetic field consists of a Gaussian 2D flux tube, slab turbulence, and a uniform field $B_0\hat{z}$. For the 2D flux tube, the potential function $a(x, y)$ is chosen as a Gaussian function:

$$a(r) = A_0 \exp\left[-\frac{r^2}{2\sigma^2}\right], \tag{2}$$

where A_0 is the central maximum value, σ determines the thickness of the Gaussian, and distance r is measured from the axis of the flux tube. Therefore, from $\mathbf{B} = \nabla \times \mathbf{A}$, we can write

$$\mathbf{b}^{2D}(r) = \frac{ra(r)}{\sigma^2}\,\hat{\theta}, \tag{3}$$

where $\hat{\theta}$ is the unit vector associated with the angular coordinate in a cylindrical coordinate system defined by the flux tube axis.

[8] Without the slab field, the field line trajectory in this model, $B_0\hat{\mathbf{z}} + \mathbf{b}^{2D}(x, y)$, has a helical orbit along a cylinder surface of constant $a(x, y)$ with a constant angular frequency $K = a(r_0)/(B_0\sigma^2) = (b^{2D}(r_0)/B_0)/r_0$, where r_0 is the starting radius. For the slab turbulence we choose the spectrum

$$P_{xx}^{slab}(k_z) = P_{yy}^{slab}(k_z) = \frac{C}{\left[1 + (k_z\lambda)^2\right]^{5/6}}, \tag{4}$$

where λ is the coherence length and C is constant.

[9] For the numerical simulations, we set the box length in the z direction as 10,000 λ and the number of grid points is $N_z = 4{,}194{,}304$. We are particularly interested in small flux ropes surrounding O-points in 2D turbulence, which are permeated by homogeneous mean and slab fields, so we keep constant the mean field (B_0), all parameters of the slab turbulence, and the width of the 2D island ($\delta b_{slab}/B_0 = 0.5$ and $\sigma = 0.5\lambda$, where $B_0 = 5$ nT and $\lambda = 0.02$ AU). These parameters roughly represent conditions in interplanetary space near Earth. In different numerical experiments we vary the strength of the 2D field - which indeed does vary in interplanetary space - by changing $b_{2D}^{\max}$. For these simulations, we define $b_{2D}^{\max}/B_0 = 0.0$, 0.5, 1.0, and 1.58 for pure slab, low B, medium B, and high B; which is equivalent to $(b_{2D}^{\max}/\delta b_{slab})^2 = 0.0$, 1.0, 4.0, and 10.0, respectively.

2.3. Particle Properties

[10] We focus on particles at three different energies as presented in Table 1. Here $r_L = \gamma m_0 v/(|q|B_0)$, and the test particles are designed to represent protons. Given our choice of B_0 (see Section 2.2), these values of the Larmor radius r_L roughly match the maximum gyroradius of such particles in interplanetary space near Earth. The energies are referred to below as high energy (1 MeV), medium energy (0.1 MeV) and low energy (20 keV).

2.4. Simulations

[11] At the initial time step, 5,000 particles are placed at $r_0 = 0.1\lambda = 0.2\sigma$, which is near the center of the Gaussian flux tube. The initial particle velocity is uniformly distributed in direction (isotropic). Because of the symmetry of the slab turbulence, the particle positions are initially at random

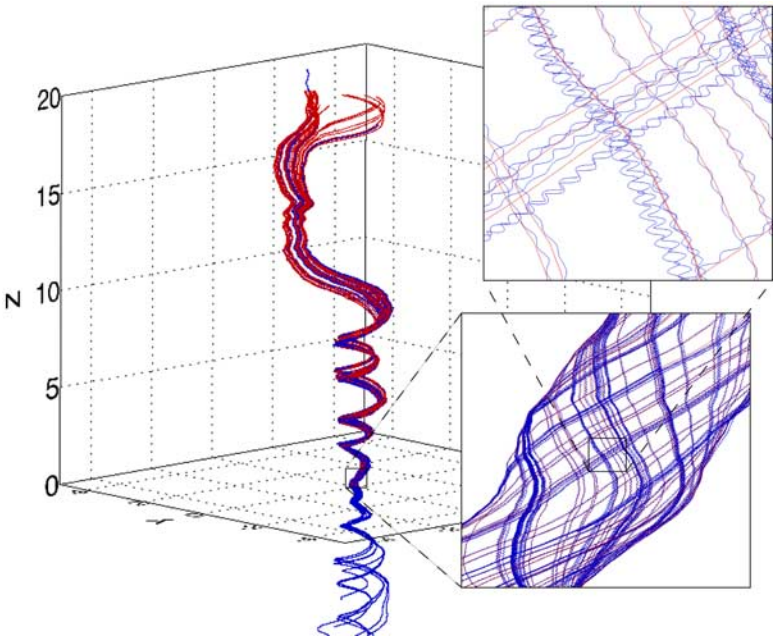

Figure 1. Illustration of 50 magnetic field lines (light red) and the trajectories of 50 particles (dark blue) with the same initial positions that start at $z = 0$, $r = 0.1\lambda$ in a mean field + Gaussian 2D field + slab turbulence. Here the parameters of the 2D field are the same as in the high B case and all particles have low E (for details see Section 2.2 and Table 1). In the main plot, while trapped, the field lines map out regular flux surfaces of the Gaussian flux tube until their escape. Note that some particles undergo resonant pitch angle scattering and move downward to $z < 0$. In the lower inset, individual guiding center motion is evident. In the inset showing the most magnified view, the gyration of individual particles is seen.

z positions for estimation of ensemble average statistics of perpendicular displacement.

[12] Particle trajectories are computed in time t by a fourth-order Runge-Kutta method with adaptive time stepping regulated by a fifth-order error estimate step.

[13] We calculate the average of the squared perpendicular displacement $\langle \Delta r^2 \rangle = \langle \Delta x^2 + \Delta y^2 \rangle$, where $\Delta x = x - x_0$ and $\Delta y = y - y_0$, and a running diffusion coefficient of the particles, given as $\widetilde{\kappa} = \langle \Delta x^2 + \Delta y^2 \rangle / (4t)$ at time t.

3. Simulation Results

[14] Figure 1 shows sample particle trajectories for low energy and high flux tube field strength (low E and high B, showing particles and field lines starting at $z = 0$ for clarity of presentation).

[15] At the coarsest spatial resolution one sees a collection of guiding centers that are initially confined to the flux surfaces of the 2D flux tube, but gradually escape (towards the top of Figure 1.) At finer spatial scales (lower inset) the individual particle trajectories become apparent, and one sees that they follow slightly different field lines. At the finest resolution (upper inset) the gyro-orbits become apparent and are the dominant feature. It is apparent that the magnetic field, and therefore the particle orbits, exhibit a multi-scale structure.

[16] Figure 2 shows mean square displacements vs. time for various particle energies and flux tube fields (top plots). These displacements, measured perpendicular to $B_0\hat{z}$, have a more complex behavior with the flux tube present. In the bottom plots, particle transport with varying 2D field and particle energy is illustrated in terms of the time-dependent running diffusion coefficient, $\widetilde{\kappa}$. It is clear that $\widetilde{\kappa}$ does not monotonically approach a time asymptotic form of the transport. For all cases that include a 2D flux tube, there is a period of time in which the rate of transport is suppressed.

[17] The left plots of Figure 2 show how low energy particles behave in flux tubes of varying strength, with other parameters fixed. The pure slab case is considered as well, and is the limit of a zero strength 2D flux tube. The time-varying features introduced by the 2D flux tubes are more prominent as the flux tube field strength increases. Based on analyses such as these, we identify four regimes of particle transport in these numerical experiments (Figure 2, top right), seen most clearly in the cases of lower energy and higher flux tube magnetic field:

[18] I. Streaming regime ($\langle \Delta r^2 \rangle \propto t^2$): the particles orbit around the field lines which are mainly confined to the 2D flux tube surface. The effects of the slab turbulence on these trajectories is small at this stage. This persists until the first peak in the diffusion coefficient plot (Figure 2, bottom left), estimated by $t = s/v$, where

$$s = \pi r_0 \sqrt{1 + \left[\frac{B_0}{b_{2D}(r_0)}\right]^2} \tag{5}$$

corresponds to a half cycle of the helical field line trajectory and v is the isotropic speed ($|\mathbf{v}|/\sqrt{3}$) of the particles, as shown in Table 1. This calculated time of the first peak agrees reasonably well with the simulation results.

[19] II. Temporary trapping regime and suppressed diffusion ($\langle \Delta r^2 \rangle \propto$ from t^0 to t^1): The particles have filled the flux tube surface and are temporarily trapped on it. The

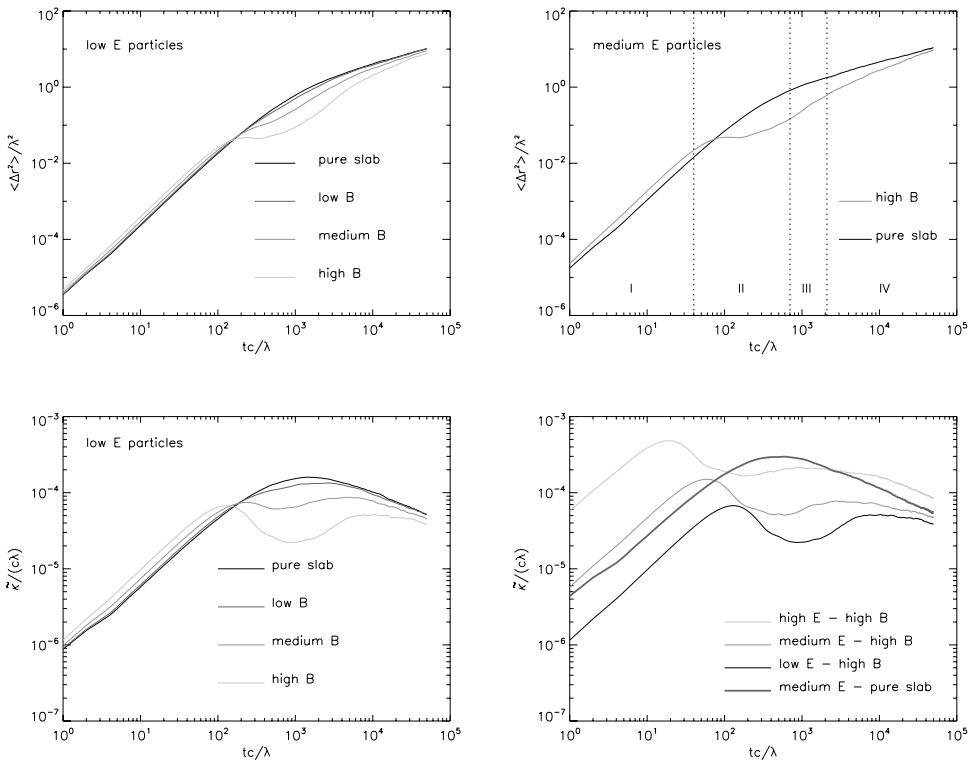

Figure 2. (top) Mean squared perpendicular displacement $\langle \Delta r^2 \rangle$ vs. time t for various cases. (bottom) Running perpendicular diffusion coefficient $\widetilde{\kappa} = \langle \Delta r^2 \rangle / (4t)$ vs. time t for various cases. There is more trapping for lower energy particles and for stronger 2D flux tubes.

gyrocenters follow an approximately helical path, and the radial coordinates of the particles begin to increase slowly. This broadening briefly reaches a slow diffusive rate of transport as the gyrocenters follow field lines which themselves are experiencing a suppressed diffusive escape from the flux tube [*Chuychai et al.*, 2005].

[20] III. Escape region ($\langle \Delta r^2 \rangle$ from t^1 to t^2): As the particle population escapes the 2D flux tube, the transport is increasingly dominated by the stronger (unsuppressed) effects of the slab turbulence. This corresponds to a super-diffusive regime (equivalent to a second free streaming regime) in which the transition to this higher rate of transport is accomplished for the entire population.

[21] IV. Asymptotic transport: Subdiffusion regime ($\langle \Delta r^2 \rangle \propto t^{1/2}$): After escape, the particles experience the full effect of the exterior turbulence. In many cases this would be an asymptotic diffusive regime. However for the present simplified model, the displacements become sub-diffusive in the exterior pure slab turbulence because of the parallel scattering [see *Qin et al.*, 2002a, 2002b; *Webb et al.*, 2006]. This final regime of transport begins at the second peak corresponding to the estimated parallel scattering time.

[22] Figure 2 includes reference curves of transport in pure slab turbulence (particle energy as labelled). For the pure slab cases we can see only two transport regimes, free-streaming at early times, followed by time-asymptotic subdiffusive transport. At very early times, free streaming within a 2D flux tube can be more rapid than in the pure slab case, causing the mean square displacement for the flux tube cases to sometimes lie above the slab case. However the temporary trapping or confinement within the flux tubes has no analog for the pure slab case, and, in this regime of time scales, particles confined by 2D flux tubes have systematically lower values of mean square perpendicular displacement.

3.1. Trapping Time

[23] Temporarily confined particles require a longer time to reach a specified mean square displacement than do the corresponding pure slab experiments. We define a trapping time as the difference in time required to attain a specified perpendicular displacement.

[24] Suppose that $f_g(t)$ and $f_s(t)$ are the mean square displacements for the Gaussian flux tube and pure slab cases respectively. It is clear that f_g must be evaluated at a later time $t + t_{trap}$ in order to attain a displacement equal to $f_s(t)$ (see f_s and f_g in the top plots of Figure 2). We define the trapping time t_{trap} by $f_g(t + t_{trap}) = f_s(t)$, where t_{trap} is uniquely defined because both functions increase monotonically. We find a fairly stable value in most of our runs after the epoch of escape begins. Most of the delay in transport in the cases with Gaussian flux tubes is experienced during the period of trapping and suppressed diffusive escape. Here we choose the high B case to find t_{trap}, shown in Table 2.

Table 2. Trapping Times

	Low E	Medium E	High E
Energy, MeV	0.02	0.10	1.00
t_{trap}, λ/c	5×10^4	9.5×10^3	3×10^3
t_{trap}, λ/v	326	139	138

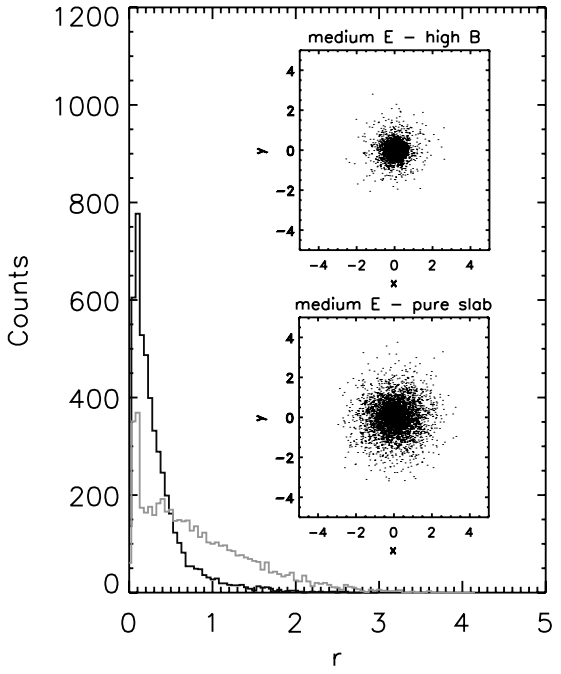

Figure 3. Example of how a 2D flux tube (the high B case) confines particles and leads to steep spatial gradients for an extended time (black histogram), in comparison with a case with no flux tube (pure slab; gray histogram). Distances are in units of λ, and r is the distance from the axis of the flux tube, which has a Gaussian potential function with $\sigma = 0.5\lambda$. Histograms show counts per 0.05 λ bin. The 5000 particles were started at t = 0 from random locations within $r = 0.1\lambda$ from the flux tube axis, and the histograms and scatter plots (insets) indicate their locations at $t = 1000\lambda/c$. The sharp gradients for the high B case correspond to dropout features in energetic ions and electrons from impulsive solar flares as observed near Earth.

3.2. Confinement and Steep Gradients

[25] To demonstrate the temporary trapping of particles in another way, Figure 3 shows the spatial distribution of 5000 particles at $t = 1000\lambda/c$, where the particles started at random locations within $r = 0.1\lambda$ from the flux tube axis at $t = 0$. In the high B case, particles are clearly inhibited from leaving the flux rope (with $\sigma = 0.5$) in comparison to the pure slab case. Thus the mechanism of field line trapping and confinement in small 2D flux tube structures, proposed as a basis for explaining dropouts [*Ruffolo et al.*, 2003; *Chuychai et al.*, 2005, 2007], is shown to also yield particle confinement and steep gradients.

4. Discussion

[26] Usually one expects that charged test particles moving in a uniform mean magnetic field with random perturbations will, after moving a few turbulence correlation lengths, experience spatial diffusion, or some other time-asymptotic transport (such as compound diffusion, or sub-diffusion.) The present numerical results show that when additional, modest perturbations in the form of closed two-dimensional flux tubes are present, the time for some particles to attain the time-asymptotic regime of spatial transport can be greatly increased. This is due to temporary trapping in the transverse magnetic topology imposed by flux tubes. Particles of lower energy that are deeply embedded in stronger flux tubes of this type are expected to most prominently display trapping, suppressed escape, and the associated delays in perpendicular transport.

[27] The effect described is the direct analog for particles of the topological trapping and suppressed diffusive escape of magnetic field lines from the vicinity of O-type neutral points in the transverse, 2D fluctuation fields [*Ruffolo et al.*, 2003; *Chuychai et al.*, 2005, 2007].

[28] The present ideas may be relevant to heliospheric phenomena such as dropouts that appear to require weaker or absent diffusion. Here we see that the trapping delays the onset of asymptotic transport, but does not prevent it, and that during this time, sharp gradients can persist, possibly appearing over a great span of heliocentric distance. To assess this idea more quantitatively in the context of dropouts, a more detailed model will have to be developed, including radial expansion, flows, and fully three dimensional effects of the inhomogeneous magnetic field in the heliosphere.

[29] **Acknowledgments.** This research was supported by the Thailand Research Fund, the Ratchadaphiseksomphot Endowment Fund of Chulalongkorn University, and NASA grants NNG05GG83G, NNG04GF81G, and NNG04GA54G.

References

Bieber, J. W., W. H. Matthaeus, C. W. Smith, W. Wanner, M. Kallenrode, and G. Wibberenz (1994), Proton and electron mean free paths: The Palmer consensus revisited, *Astrophys. J.*, *420*, 294.

Chuychai, P., D. Ruffolo, W. H. Matthaeus, and G. Rowlands (2005), Suppressed diffusive escape of topologically trapped magnetic field lines, *Astrophys. J.*, *633*, L49.

Chuychai, P., D. Ruffolo, W. H. Matthaeus, and J. Meechai (2007), Trapping and diffusive escape of field lines in two-component magnetic turbulence, *Astrophys. J.*, *659*, 1761.

Fisk, L. A. (1996), Motion of the footpoints of heliospheric magnetic field lines at the Sun: Implications for recurrent energetic particle events at high heliographic latitudes, *J. Geophys. Res.*, *101*, 15,547.

Giacalone, J., J. R. Jokipii, and J. E. Mazur (2000), Small-scale gradients and large-scale diffusion of charged particles in the heliospheric magnetic field, *Astrophys. J.*, *532*, L75.

Jokipii, J. R. (1966), Cosmic-ray propagation. I. Charged particles in a random magnetic field, *Astrophys. J.*, *146*, 480.

Jokipii, J. R., J. Kóta, and J. Giacalone (1993), Perpendicular transport in 1- and 2-dimensional shock simulations, *Geophys. Res. Lett.*, *20*, 1759.

Jones, C., J. R. Jokipii, and M. G. Baring (1998), Charged-particle motion in electromagnetic fields having at least one ignorable spatial coordinate, *Astrophys. J.*, *509*, 238.

Matthaeus, W. H., P. C. Gray, D. H. Pontius Jr., and J. W. Bieber (1995), Spatial structure and field-line diffusion in transverse magnetic turbulence, *Phys. Rev. Lett.*, *75*, 2136.

Mazur, J. E., G. M. Mason, J. R. Dwyer, J. Giacalone, J. R. Jokipii, and E. C. Stone (2000), Interplanetary magnetic field line mixing deduced from impulsive solar flare particles, *Astrophys. J.*, *532*, L79.

McKibben, R. B., C. Lopate, and M. Zhang (2001), Simultaneous observations of solar energetic particle events by IMP 8 and the Ulysses COSPIN high energy telescope at high solar latitudes, *Space Sci. Rev.*, *97*, 257.

Parker, E. N. (1965), The passage of energetic charged particles through interplanetary space, *Planet. Space Sci.*, *13*, 949.

Qin, G., W. H. Matthaeus, and J. W. Bieber (2002a), Subdiffusive transport of charged particles perpendicular to the large scale magnetic field, *Geophys. Res. Lett.*, *29*(4), 1048, doi:10.1029/2001GL014035.

Qin, G., W. H. Matthaeus, and J. W. Bieber (2002b), Perpendicular transport of charged particles in composite model turbulence: Recovery of diffusion, *Astrophys. J.*, *578*, L117.

Ruffolo, D., W. H. Matthaeus, and P. Chuychai (2003), Trapping of solar energetic particles by the small-scale topology of solar wind turbulence, *Astrophys. J.*, *597*, L169.

Webb, G. M., G. P. Zank, E. K. Kaghashvili, and J. A. Le Roux (2006), Compound and perpendicular diffusion of cosmic rays and random walk of the field lines. I. Parallel particle transport models, *Astrophys. J.*, *651*, 211.

J. W. Bieber, P. Chuychai, W. H. Matthaeus, and J. Minnie, Department of Physics and Astronomy and Bartol Research Institute, University of Delaware, 217 Sharp Lab, Newark, DE 19716-4793, USA. (john@bartol.udel.edu; paeng@bartol.udel.edu; whm@udel.edu; minnie@bartol.udel.edu)

P. Tooprakai, Department of Physics, Faculty of Science, Chulalongkorn University, Bangkok 10330, Thailand. (paisan@astro.phys.sc.chula.ac.th)

D. Ruffolo, Department of Physics, Faculty of Science, Mahidol University, Bangkok 10400, Thailand. (david_ruffolo@yahoo.com)